2024 年度　博士論文

Search for drugs that inhibit pyroptosis-driven inflammation and analysis of their mechanisms of action

パイロトーシスを介した炎症応答を抑える薬剤の探索と作用機序の解析

創成薬学専攻
生体応答制御学分野
潘　逸羲

Abstract

Humans are constantly exposed to various industrial, environmental, and endogenous particles that result in inflammatory diseases. For example, the inhalation of particles comprising crystalline silica, such as yellow dust and PM2.5, results in pneumoconiosis and allergies. Moreover, metabolic crystalline particles like monosodium urate (MSU) crystals, which are generated in the body owing to overnutrition, cause gout. After being engulfed by immune cells, viz. macrophages, such particles are present in phagosomes. Phagosomes containing particles mature into phagolysosomes through fusing with lysosomes. Eventually, particles lead to phagolysosomal dysfunction, inducing pyroptosis, a form of cell death accompanied by the release of inflammatory mediators, including members of the interleukin (IL)-1 family. Phagolysosomal dysfunction results in the activation of the nod-like receptor family pyrin domain containing 3 (NLRP3) inflammasome, an immune complex that induces cell death and release of IL-1β upon exposure to various external stimuli. However, several particles, such as silica particles (SPs) and MSU crystals, still induce cell death and release of other inflammatory mediators, such as IL-1α, even if the NLRP3 inflammasome-associated response is inhibited; this indicates that such inhibition is not always effective in treating diseases induced by particles. Therefore, the discovery of drugs suppressing particle-induced NLRP3-independent pyroptosis is warranted.

In this study, I screened the compounds that can inhibit SP-induced cell death and IL-1α release using a high-content imaging-based system. Furthermore, I used RAW264.7, a mouse macrophage cell line which lacks the NLRP3 inflammasome, to avoid the effect of NLRP3 inflammasome-mediated response. As a result, I found that several Src family kinase (SFK) inhibitors, including dasatinib, effectively suppressed

SP-induced cell death and IL-1α release in both RAW264.7 cells and mouse primary macrophages. Furthermore, dasatinib also suppressed pyroptosis induced by other particles, such as yellow dust and MSU crystals. However, it did not suppress pyroptosis induced by non-particles, such as adenosine triphosphate, indicating that dasatinib specifically suppresses particle-induced pyroptosis. Mechanistically, dasatinib reduced SP-induced phagolysosomal dysfunction without affecting the phagocytosis of SPs. Additionally, dasatinib administration strongly suppressed the increase in IL-1α levels and neutrophil counts in the lungs after intratracheal SP administration. In conclusion, dasatinib suppresses particle-induced pyroptosis and can be used to treat relevant inflammatory diseases.

Contents

1. Introduction

Pyroptosis is derived from the Greek roots “pyro” and “ptosis”. “pyro” means fire, and “ptosis” means falling, indicating that pyroptosis is pro-inflammatory programmed cell death. Pyroptosis typically involves the rupture of cell membranes and the release of pro-inflammatory cytokines, such as members of the interleukin-1 (IL-1) family, resulting in the induction of inflammation [1]. Pyroptosis plays a central role in the immune response, protecting the host from pathogen invasion. However, excessive induction of pyroptosis can lead to aberrant inflammatory responses, leading to various inflammatory diseases [2]. For instance, many studies have reported that particle irritants-induced pyroptosis is involved in the pathogenesis of several inflammatory diseases. The inhalation of particles comprising crystalline silica, such as yellow dust and PM2.5, results in pneumoconiosis and allergies [3, 4]. Amorphous silica can also lead to pneumoconiosis [5]. Industrial materials such as asbestos and carbon nanotubes lead to pneumoconiosis and mesothelioma, whereas titanium dioxide causes dermatitis and enteritis [3, 6, 7]. In addition, metabolic crystalline particles, including monosodium urate (MSU), cholesterol, and calcium oxalate crystals, generated in the body owing to overnutrition, cause gout, arteriosclerosis, and nephritis, respectively [8-10]. Harmful particles also include protein aggregates, such as amyloid-β deposits, which lead to Alzheimer’s disease with aging [11]. Therefore, drugs that prevent pyroptosis can potentially treat inflammatory diseases induced by particle irritants.

Invading or intrinsic particles are engulfed by immune cells such as macrophages. Phagosomes containing foreign substances undergo maturation by sequentially recruiting various proteins, including Rab guanosine triphosphatase, and eventually fusing with lysosomes to form phagolysosomes, which digest the engulfed

substances [12]. However, particles with sharp crystal structures and/or particular surface properties destabilize the phagolysosomal membrane, resulting in the leakage of its contents [13]. Phagolysosomal dysfunction activates the nod-like receptor family pyrin domain containing 3 (NLRP3), an intracellular pattern recognition receptor, which senses microbial invasion [14]. Upon activation, NLRP3 forms a protein complex (termed inflammasome) with the adaptor molecule apoptosis-associated speck-like protein containing a caspase recruitment domain and caspase-1 [14]. Caspase-1 induces the maturation of cytokines of the IL-1 family, such as IL-1β and IL-18, and gasdermin D, which form pores in the plasma membrane and induce cytokine release and subsequent cell death [14]. However, recent studies suggest that targeting NLRP3 inflammasome-associated responses are insufficient in treating inflammatory diseases induced by particles, such as silica particles (SPs) and MSU crystals, because these particles continue to induce cell death and inflammatory mediator release in the absence of NLRP3 or gasdermin D [4, 6, 15-18]. IL-1α is an important molecule among those released during NLRP3-independent pyroptosis owing to its proinflammatory effects by binding to the same receptor as IL-1β. Several animal studies have reported that IL-1α plays critical roles in the development of particle-induced inflammatory diseases [4, 6, 15, 16, 18]. However, preventing NLRP3-independent cell death and the resultant release of inflammatory mediators remains a key challenge during the development of efficient treatment strategies for inflammatory diseases induced by particle irritants.

In a previous study, our laboratory proposed the natural compound oridonin as an effective drug candidate for treating particle-induced inflammatory diseases [18]. Oridonin suppressed particle-induced NLRP3-independent cell death and IL-1α release and attenuated NLRP3-independent lung inflammation in a mouse model of

silicosis. However, oridonin and its derivatives are still not clinically approved. In the present study, I performed a library screening to identify compounds that can suppress particle-induced cell death and IL-1α release with the intent of drug repositioning. Consequently, I identified dasatinib, a clinically approved drug, as a potential therapeutic agent for particle-induced inflammatory diseases.

2. Materials and methods:

2.1. Reagents and cell line

Pfizer and FDA-approved drug libraries were kindly provided by the Center for Supporting Drug Discovery and Life Science Research, Graduate School of Pharmaceutical Sciences, Osaka University. Plain and fluorescent amorphous SPs (Sicastar; 500, 1,500, and 3,000 nm in diameter) were purchased from MicroMod (Rostock, Germany). Chemi-Lumi One Super and MSU were purchased from Nacalai Tesque (Kyoto, Japan). Gobi Kosa dust (yellow dust) was purchased from the National Institute for Environmental Studies (Ibaraki, Japan). Adenosine triphosphate (ATP) was purchased from Enzo Life Sciences (Farmingdale, NY, United States). DRAQ7 was purchased from Biostatus (Loughborough, United Kingdom). Bosutinib, cytochalasin D (Cyto D), dasatinib, L-leucyl-L-leucine methyl ester (LLoMe), PD-161570, and iFluor-488-conjugated phalloidin were purchased from Cayman Chemical Company (Ann Arbor, Michigan, United States). PD-166285 dihydrochloride was purchased from Tocris Biosciences (Abingdon, United Kingdom). Dasatinib hydrochloride for in vivo experiments was purchased from MedChem Express (Monmouth Junction, NJ, United States). Hoechst 33342, LysoTracker Deep Red, and ProLong Gold antifade Mountant were purchased from Thermo Fisher Scientific (Waltham, MA, United States). DRAQ5 and the enzyme-linked immunosorbent assay (ELISA) kit for mouse IL-1β were purchased from BioLegend (San Diego, CA, United States). Can Get Signal Immunoreaction Enhancer Solution was purchased from Toyobo (Osaka, Japan). Immobilon Forte Western horseradish peroxidase (HRP) substrate was purchased from Merck Millipore (Burlington, MA, United States). Collagenase (crude type) was purchased from FUJIFILM Wako Pure Chemical Corporation (Osaka, Japan). Lipopolysaccharide

(LPS) from Escherichia coli O111:B4 and DNase I were purchased from Sigma-Aldrich (St. Louis, MO, United States). The ELISA kits for mouse chemokine (C-X-C motif) ligand (CXCL) 1 and mouse and human IL-1α and IL-1β were purchased from R&D Systems (Minneapolis, MN, United States). The cytotoxicity lactate dehydrogenase (LDH) assay kit (WST) was purchased from Dojindo Laboratories (Kumamoto, Japan).

RAW264.7, a mouse macrophage cell line, and THP-1, a human monocytic cell line, were purchased from Riken (Ibaraki, Japan).

2.2. Antibodies

Anti-phospho-Src family (D49G4), anti-RAB5A, member RAS oncogene family (RAB5A) (E6N8S), HRP-conjugated anti-mouse IgG, and HRP-conjugated anti-rabbit IgG antibodies were purchased from Cell Signaling Technology (Danvers, MA, United States). Anti-lysosome-associated membrane protein-1 (LAMP-1) (1D4B) and anti-phosphatidylinositol 4,5-bisphosphate (PIP2) (2C11) antibodies were purchased from Abcam (Cambridge, United Kingdom). Anti-actin antibody (C-11) was purchased from Santa Cruz Biotechnology (Dallas, TX, United States). Alexa Fluor-labeled secondary antibodies and HRP-conjugated anti-goat IgG (H + L) antibodies were purchased from Thermo Fisher Scientific. The Alexa Fluor 488-conjugated anti-mouse CD11b (M1/70), Pacific Blue-conjugated anti-mouse CD45 (30-F11), Alexa Fluor 647-conjugated anti-mouse Ly-6G (1A8) and phycoerythrin-cyanine7-conjugated anti-mouse Ly-6C (HK1.4) antibodies were purchased from BioLegend.

2.3. MSU crystal formation

The pH of 250 mL of sterile water was adjusted to pH 6.8 by adding hydrochloric acid. MSU (750 mg) was then added, and the mixture was stirred at 60°C for 3–5 days. After passing through a 0.22 μm filter, the supersaturated urate solution was left standing at room temperature for 3–8 weeks. The resulting crystals were harvested by centrifugation at 8000 × *g* for 5 min, washed three times with 70% ethanol, and dried at 60°C for several days.

2.4. Mice

C57BL/6J mice (5-week-old females) were purchased from Japan SLC, Inc. (Shizuoka, Japan). During the experimental period, all mice were housed in standard cages in a temperature-controlled room under a 12-h light/dark cycle at the animal care facility of the Graduate School of Pharmaceutical Sciences, Osaka University. Mice were provided ad libitum access to standard laboratory mouse chow and drinking water. All animal experiments were approved by the Animal Care and Use Committee of the Graduate School of Pharmaceutical Sciences at Osaka University.

2.5. Screening of compounds that can inhibit particle-induced cell death and IL-1α release

RAW264.7 cells were seeded at a density of 3.5×10^4 cells/well into glass-bottom 96-well plates and primed with LPS (100 ng/ml) for 16 h in Eagle's minimal essential medium (Nacalai Tesque) supplemented with 10% fetal calf serum (FCS), penicillin (100 U/ml), streptomycin (100 μg/ml), and non-essential amino acids (Nacalai Tesque, 100x). Cells were pretreated with each compound (5 μM) from the Pfizer- and FDA-approved drug libraries for 30 min and then stimulated with SPs

(500 nm in diameter, 500 μg/ml) in the presence of DRAQ7 (2 μM) and Hoechst 33342 (1 μg/ml) for 2 h. After collecting the supernatants, the cells were fixed with 4% paraformaldehyde for 15 min and then rinsed with ice-cold phosphate-buffered saline. Images were acquired from four fields per well using the Cell Voyager CV8000 High Content Screening System (Yokogawa Electric Corp., Tokyo, Japan). Hoechst 33342-positive and DRAQ7-negative cells and Hoechst 33342 and DRAQ7 double-positive cells were considered viable and dead cells, respectively. The cell death rate was calculated by dividing the number of dead cells by the total number of cells using CellPathfinder software (Yokogawa Electric Corp.). IL-1α levels in the cell culture supernatants were measured using ELISA, as described below. A test compound was defined as a hit if the mean percentage inhibition of cell death and IL-1α release was >50%.

2.6. Macrophage preparation and stimulation

To prepare bone marrow-derived macrophages (BMDMs), mouse bone marrow cells were cultured with macrophage colony-stimulating factor (10 ng/ml) in RPMI 1640 medium (Nacalai Tesque) supplemented with 10% FCS, penicillin, and streptomycin. 5 days after culture initiation, cells were collected and used as BMDMs. The BMDMs were seeded at a density of 4×10^5 cells/well in 48-well plates and primed with LPS (200 ng/ml) in RPMI 1640 medium supplemented with 10% FCS for 6 h. The primed cells were pretreated with bosutinib (20 μM), Cyto D (20 μM), dasatinib (20 μM), PD-161570 (20 μM), or PD-166285 (20 μM) for 30 min and then stimulated with SPs (500, 1,500 or 3,000 nm in diameter, 300 μg/ml), MSU (300 μg/ml), yellow dust (500 μg/ml), or ATP (3 mM) for 2 h or with LLoMe (0.5 mM) for 3 h.

THP-1 cells were seeded at a density of 4×10^5 cells/well in 48-well plates and induced for macrophage differentiation by culturing them with phorbol 12-myristate 13-acetate (10 ng/ml) in RPMI 1640 medium supplemented with 10% FCS for 1 day, followed by an additional 2 days of culture in phorbol 12-myristate 13-acetate-free medium. THP-1 cells were primed with LPS (50 ng/ml) in RPMI 1640 medium supplemented with 10% FCS for 16 h. The primed cells were pretreated with dasatinib (20 μM) for 30 min and then stimulated with SPs (1,500 nm in diameter, 500 μg/ml) for 4 h.

The supernatants from each culture condition were collected after centrifuging the samples at 440 ×g and 4°C for 5 min. The supernatants and cell samples were analyzed.

2.7. Cell viability measurement

Cell viability was determined by measuring LDH activity in the culture supernatants using the cytotoxicity LDH assay kit (WST) according to the manufacturer's instructions.

2.8. Immunoblotting

Cell samples were washed and lysed with 30 μl of the lysis buffer containing 62.5 mM Tris–HCl (pH 6.8 at 25°C), 2% (w/v) sodium dodecyl sulfate, 10% (v/v) glycerol, 0.01% (w/v) bromophenol blue, and 42 mM dithiothreitol. Samples were then processed for immunoblotting using a previously described method [19]. Each protein was probed with the appropriate antibodies listed in the subsection "Antibodies," and the blots were visualized using Immobilon Forte Western HRP Substrate (Merck Millipore) or Chemi-Lumi One Super (Nacalai Tesque).

Immunoreactive bands were detected using FUSION Solo S (Vilber Lourmat, Collégien, France) and quantified using the ImageJ software bundled with 64-bit Java 8. (Version 1.53t) (National Institutes of Health, MD, United States).

2.9. Observation of particle uptake by BMDMs

BMDMs were cultured on coverslips and primed with LPS (200 ng/ml) for 6 h. Further, they were pretreated with Cyto D (20 μM) or dasatinib (20 μM) for 30 min and stimulated with fluorescent SPs (1,500 nm in diameter, 20 μg/ml) for 2 h. The stimulated cells were fixed with 4% paraformaldehyde for 15 min and permeabilized with digitonin (50 μg/ml) for 15 min. The membrane-permeabilized cells were stained with iFluor-488-conjugate phalloidin (1000-fold dilution) and DRAQ5 (200 μM) for 30 min. Images were obtained using the Cell Voyager CV8000 High Content Screening system, and the number of phagocytosed SPs per cell was counted using the CellPathfinder software.

2.10. Immunocytochemistry

BMDMs were cultured on coverslips and fixed with 3% paraformaldehyde. Immunocytochemistry was performed as described previously [18]. Samples were visualized under an inverted fluorescence microscope (DMI6000B; Leica Microsystems, Wetzlar, Germany) and photographed using the Application Suite X software imaging system (Leica Microsystems).

2.11. Induction of lung inflammation

Mice were randomly divided into four groups and anesthetized via isoflurane inhalation. The groups received different treatments as follows: 1) intratracheal

administration of phosphate-buffered saline; 2) intratracheal SP administration (100 mg/kg); 3) intratracheal SP administration (100 mg/kg) in combination with intragastric dasatinib administration (30 mg/kg); and 4) intratracheal administration of SP (100 mg/kg) in combination with dasatinib (10 mg/kg). Bronchoalveolar lavage (BAL) fluid was collected 12 h after the intratracheal administration of SPs. Subsequently, 1 ml of phosphate-buffered saline was flushed into the lungs, with a recovery of approximately 700 μl of BAL fluid. The remaining lung tissues were used for isolating lung leukocytes as described below. In separate experiments, the lungs were collected 12 h after the intratracheal administration of SPs for histological analysis.

2.12. Isolation of lung leukocytes

Lung tissues were minced using a pair of scissors and subsequently digested with collagenase (2 mg/ml) and DNase I (100 μg/ml) in RPMI 1640 medium supplemented with 10% FCS with continuous stirring at 37°C for 60 min. The suspended cells were centrifuged at a density-gradient of 40%–80% (v/v) Percoll. Cells (lung leukocytes) were collected from the interface, washed, and then used in further experiments.

2.13. Flow cytometric analysis

BMDMs were stained with LysoTracker Deep Red according to the manufacturer's instructions. Lung leukocytes were stained with antibodies against mouse CD11b, CD45, Ly-6C, Ly-6G, according to the manufacturer's instructions. $CD45^{+}$ $CD11b^{+}$ Ly-$6C^{med}$ Ly-$6G^{high}$ cells were identified as neutrophils [18]. The data was acquired using a flow cytometer (CytoFLEX; Beckman Coulter, Brea, CA,

United States) and analyzed using the FlowJo software (TreeStar, Ashland, OR, United States).

2.14. Histological analysis

The mouse lungs were fixed for 24 h with 10% formalin and embedded in paraffin. Five-micrometer sections of the mouse lungs were stained with hematoxylin and eosin and observed under the BZ-X800 automated high-resolution microscope (Keyence, Osaka, Japan) with an analysis application.

2.15. ELISA

Mouse CXCL1, mouse and human IL-1α and IL-1β levels in the culture supernatants and BAL fluid were measured using ELISA kits, according to the manufacturer's instructions.

2.16. Statistical analyses

All data was calculated using GraphPad Prism 8.0 software (Boston, MA, United States). One-way analysis of variance and the Tukey–Kramer post hoc test were performed for multiple group comparisons. Statistical significance was set at a *P*-value of <0.05.

3. Results:

3.1. Dasatinib suppresses particle-induced pyroptosis in macrophages

RAW264.7 cells are a macrophage cell line with impaired apoptosis-associated speck-like protein containing a caspase recruitment domain expression and negligible effects on the NLRP3 inflammasome [20]. These cells were used to identify inhibitors against particle-induced NLRP3 inflammasome-independent pyroptosis. Candidate drugs were screened by elucidating whether the treatment of LPS-primed RAW264.7 cells with the test compounds before SP stimulation suppressed cell death and IL-1α release. SP-induced cell death was determined using CellVoyager CV8000, which allows high-throughput imaging-based screening (Figure 1A). Two nuclear staining dyes, Hoechst 33342 and DRAQ7, were used to determine cell viability. Hoechst 33342 was used to stain the cell nuclei, whereas DRAQ7, a membrane-impermeable dye, was used to stain the nuclei of dead cells. Accordingly, Hoechst 33342-positive and DRAQ7-negative cells and Hoechst 33342 and DRAQ7 double-positive cells were considered viable and dead cells, respectively. Simultaneously, IL-1α levels in the culture supernatants were also measured. Screening of 1,240 compounds present in the Pfizer- and FDA-approved libraries identified two anticancer drugs, bosutinib and dasatinib, which suppressed SP-induced cell death and IL-1α release (Table 1 and Figures 1B, C). Similar results were obtained for PD-161570, PD-166285, PD-173952, and PD-407824. Interestingly, all the drug candidates target Src family kinases (SFKs), well-known signaling factors involving various cellular functions, including the induction of inflammatory responses, cell proliferation, cell differentiation, and metabolism [21, 22].

Further, mouse primary macrophages were used to validate the effects of bosutinib, dasatinib, PD-161570, and PD-166285. PD-173952 and PD-407824 were

excluded because they are not approved yet and exhibit relatively weak suppressive effects against SP-induced pyroptosis. Moreover, I confirmed that dasatinib exhibited the most potent inhibition of SFK activation, followed by PD-161570, while bosutinib and PD-166285 had the weakest effects (data not shown). To assess whether these drugs inhibit SP-induced macrophage pyroptosis, I measured IL-1β and LDH release as indicators of pyroptosis, in addition to IL-1α release. LDH is released when the plasma membrane ruptures and is often used to measure the incidence of lytic cell death, including pyroptosis [23]. All the drug candidates significantly suppressed SP-induced cell death accompanied by IL-1α and IL-1β release in BMDMs (Figures 2A-C). Since dasatinib is clinically well-studied [24], it was used as a representative of these candidates in subsequent experiments. I investigated whether dasatinib effectively suppresses SP-induced pyroptosis in human cells. Dasatinib successfully suppresses SP-induced cell death accompanied by IL-1α and IL-1β release in phorbol 12-myristate 13-acetate-treated macrophage-like THP-1 cells (Figures 2D-F). Furthermore, dasatinib did not affect the viability of BMDMs during the 12 h treatment at concentrations required to inhibit SP-induced pyroptosis (Figure 2G). Therefore, dasatinib and other SFK inhibitors effectively suppressed particle-induced pyroptosis.

3.2. Increase in active SFK levels enhances particle-induced cell death

Macrophages were initially primed with LPS to induce intracellular IL-1α and IL-1β expression by activating toll-like receptor (TLR) 4. However, TLR4 increases the levels of active SFKs by enhancing their transcription and phosphorylation at Tyr416 [25, 26]. Thus, I determined whether SFKs mediate particle-induced cell death without priming. As a result, dasatinib significantly

suppressed SP-induced cell death in BMDMs even without LPS priming, although the unprimed cells did not release IL-1α and IL-1β upon SP stimulation (Figures 3A-C). Immunoblotting revealed the phosphorylation of SFKs at Tyr416 (phosphorylated SFKs; p-SFKs) in unprimed BMDMs (Figures 3D, E). Furthermore, LPS priming significantly enhanced SP-induced cell death of BMDMs and increased p-SFK levels. Interestingly, dasatinib decreased SP-induced cell death rates and p-SFK levels in LPS-primed BMDMs to levels comparable to those observed in dasatinib-treated unprimed BMDMs. SP stimulation tended to slightly decrease p-SFK levels in unprimed BMDMs but did not affect those in LPS-primed cells. To summarize, these results suggest that basal p-SFK levels can mediate particle-induced cell death, and an increase in p-SFK levels via priming is associated with particle-induced cell death.

3.3. Dasatinib suppresses particle-induced pyroptosis of various sizes or materials

Particles exhibit size-dependent variations in inflammatory properties and cytotoxicity [27-29]. I evaluated the suppressive effects of dasatinib on pyroptosis induced by SPs of different sizes. An actin-polymerization inhibitor, Cyto D, almost completely suppressed cell death accompanied by IL-1α and IL-1β release in BMDMs induced by SPs with diameters of 500, 1,500, and 3,000 nm (Figures 4A-C), suggesting these SPs were incorporated via actin-dependent phagocytosis. In addition, dasatinib significantly suppressed the cell death of BMDMs accompanied by IL-1α and IL-1β release induced by SPs, the efficacy of which varied with SP size (Figures 4A-C).

Furthermore, dasatinib suppressed cell death and IL-1α and IL-1β release induced by yellow dust, which contains crystalline silica, and MSU crystals (Figures

4D-F) indicating that it suppresses pyroptosis induced by particles of various materials.

In addition, I determined whether dasatinib suppresses pyroptosis induced by external stimuli other than particles. ATP activates the NLRP3 inflammasome by inducing mitochondrial dysfunction, resulting in pyroptosis [14]. However, dasatinib did not suppress ATP-induced cell death and IL-1α and IL-1β release (Figures 4D-F). Therefore, the suppressive effects of dasatinib on pyroptosis are selective and are strongly exhibited during particle-induced pyroptosis.

3.4. Dasatinib suppresses particle-induced phagolysosomal dysfunction without affecting phagocytosis

Next, I further attempted to elucidate the mechanism underlying the effect of dasatinib on particle-induced cellular responses. SFKs regulate Fcγ receptor-mediated phagocytosis [30]. Therefore, I investigated whether dasatinib inhibits the phagocytosis of SPs by BMDMs. BMDMs were visualized by staining the nuclei and filamentous actin with fluorescent dyes after stimulation with fluorescent SPs and counting the number of SPs incorporated into the cytoplasm under a microscope (Figure 5A). Cyto D markedly decreased the number of incorporated SPs; whereas, dasatinib had no effects on SP phagocytosis (Figure 5B). Therefore, the suppression of particle-induced pyroptosis by dasatinib is unlikely to be caused by the inhibition of phagocytic activity against particles.

Flow cytometric analysis of BMDMs stained with LysoTracker Deep Red, an acidotropic fluorescent dye which labels acidic organelles, including phagolysosomes, was performed to elucidate whether dasatinib suppresses SP-induced phagolysosomal dysfunction [18]. The stimulation of BMDMs with SPs decreased the fluorescence

intensity of LysoTracker Deep Red, indicating loss of the interior acidity of the phagolysosomes owing to leakage of their contents (Figures 5C, D). Dasatinib significantly decreased the population of LysoTracker Deep Red-negative cells among SP-stimulated cells. Thus, dasatinib was found to suppress particle-induced phagolysosomal dysfunction.

Furthermore, I elucidated whether dasatinib reduced lysosomal dysfunction and subsequent pyroptosis induced by the lysosomotropic compound LLoMe. LLoMe accumulates in the lysosomes and is processed by the lysosomal thiol protease dipeptidyl peptidase I [31]. This process results in lysosomal dysfunction. Dasatinib significantly suppressed LLoMe-induced cell death and IL-1α and IL-1β release (Figures 6A-C). Furthermore, it decreased the population of LysoTracker Deep Red-negative cells among LLoMe-stimulated cells (Figures 6D, E). Therefore, these results indicate that dasatinib suppressed pyroptosis by preventing phagolysosomal and lysosomal dysfunction.

3.5. Phosphorylated SFKs accumulate around particle-engulfed phagosomes

Based on the findings of the present study, SFKs potentially mediate the dysfunction of SP-containing phagolysosomes. SFKs, including Src, Fyn, Lyn, and Yes, are recruited to actin-rich phagocytic cups during Fcγ receptor-mediated phagocytosis [32]. Therefore, I performed immunofluorescence analysis of BMDMs to investigate the spatio-temporal activity of SFKs after the cells phagocytosed particles. In the initial stages of phagocytosis, PIP2 accumulates and initiates actin polymerization to extend the pseudopod and engulf the target (e.g., particles) [33]. Without SP stimulation, both PIP2 and p-SFKs were distributed throughout the cytoplasm of LPS-primed BMDMs (Figure 7). SPs were surrounded by PIP2 in

BMDMs 15 min after SP stimulation. Furthermore, p-SFKs accumulated around some PIP2-surrounded SPs. Dasatinib abolished p-SFK signals but did not affect the intensity or distribution of the PIP2 signals. These observations suggest that p-SFKs accumulate around the phagosomes engulfing particles during the initial stages of phagocytosis.

Next, I stained p-SFKs with an early phagosome marker, RAB5A, 30 min after SP stimulation. I observed RAB5A-positive vesicles in the cytoplasm of BMDMs without SP stimulation (Figure 8). Most of the engulfed SPs were surrounded by RAB5A, and some of the RAB5A-surrounded SPs were also surrounded by p-SFK. Dasatinib did not influence the intensity or distribution of RAB5A signals. Furthermore, I performed immunostaining for LAMP-1, a lysosomal membrane protein used as a marker for late phagosomes and phagolysosomes [12]. I detected LAMP-1-positive vesicles in the cytoplasm of BMDMs without SP stimulation (Figure 9). 30 min after stimulation, SPs were surrounded by LAMP-1, indicating that SP-engulfed phagosomes matured on fusing with lysosomes. However, LAMP-1 was not detected around p-SFK-surrounded SPs. Dasatinib did not affect LAMP-1 distribution after SP stimulation. In summary, p-SFKs may act on particle-engulfed phagosomes mainly during the early stages of maturation.

3.6. Dasatinib treatment alleviates particle-induced lung inflammation

Finally, I evaluated the anti-inflammatory effects of dasatinib on SP-induced lung inflammation in mice. In this model, intratracheally administered SPs induce IL-1α release from pulmonary macrophages in an NLRP3-independent manner, resulting in neutrophil recruitment and inflammation [18]. Dasatinib is an orally administered drug. I also tested topical treatment of the lung with dasatinib by its intratracheal

administration. Both, intragastric and intratracheal administrations of dasatinib suppressed SP-induced lung inflammation. Dasatinib administrations via these routes significantly decreased IL-1α and IL-1β levels in the BAL fluid of mice after the intratracheal administration of SPs (Figures 10A, B). Furthermore, dasatinib administration through both routes suppressed the levels of a neutrophil chemoattractant, CXCL1, and decreased the number of neutrophils in the mouse lungs after SP administration, although the inhibitory effect was stronger with intratracheal administration than that with intragastric administration (Figures 10C-E). Consistent with these findings, histological analysis revealed that both dasatinib treatment routes suppressed immune cell infiltration into the lungs after SP administration (Figure 10F). In summary, dasatinib effectively suppressed particle-induced NLRP3-independent lung inflammation.

4. Discussion:

As far as is known, I demonstrated for the first time that the FDA-approved drug dasatinib suppresses particle-induced cell death and IL-1α release, both of which occur even in the absence of the NLRP3 inflammasome [18]. A previous study reported that c-Src^{Y527F} (a constitutively active form of c-Src)-transduced murine embryonic fibroblasts become increasingly sensitive to drug-induced cell death, triggering permeabilization of the lysosomal membrane [34]. In addition, c-Src inhibition decreases *Mycobacterium tuberculosis*-induced lysosomal destabilization [35]. Therefore, dasatinib-targeted SFKs may promote particle-induced phagolysosomal membrane destabilization. Interestingly, p-SFKs accumulated around the phagocytic cups formed immediately after the phagocytosis of particles and persisted even after becoming early phagosomes (Figure 7, 8, 11). SFKs activate acid sphingomyelinase (ASM), a lysosomal ceramide-producing enzyme [36], which is present in early phagosomes [37]. When activated, ASM converts membrane sphingomyelin to ceramide, which is then converted to sphingosine by ceramidase [38]. The accumulation of sphingosine enhances membrane permeabilization in a detergent-like manner [39]. Interestingly, ASM inhibitors inhibit SP-induced cell death [40, 41]. Therefore, ASM may function as a downstream factor of dasatinib-targeted SFKs to facilitate the membrane destabilization of phagosomes and/or phagolysosomes that engulf particles. Furthermore, dasatinib-targeted SFKs may act on lysosomal ASM, thereby enhancing the destabilization of the lysosomal membrane induced by non-particle agents, such as LLoMe.

In the present study, p-SFKs accumulated around SPs surrounded by RAB5A (Figure 8, 11). However, LAMP-1 levels around SPs surrounded by p-SFKs were negligible (Figure 9, 11). Therefore, it is presumed that dasatinib-targeted SFKs act on

the membranes of particle-containing phagosomes only at the early stage of maturation; however, whether p-SFKs are dispersed, dephosphorylated, or degraded after the maturation of phagosomes into phagolysosomes remains unclear. Alternatively, p-SFK-accumulated phagosomes are vulnerable and immediately degrade after fusion with lysosomes. In my study, p-SFK-accumulated phagolysosomes were not detected under the experimental conditions. Therefore, further studies are warranted on p-SFKs recruitment after engulfing particles and their subsequent fate. These studies will help explain why p-SFKs are selectively recruited to certain phagosomes.

A previous study showed that immune cells recognize SPs of different sizes via distinct receptors [28]. Furthermore, even when particles of different sizes are recognized by the same receptor, they may activate different signaling pathways [28]. In my study, dasatinib only partially suppressed the pyroptosis induced by the SPs with a 3,000 nm diameter. Therefore, pyroptosis induced by SPs with a 3,000 nm diameter may be mediated by SFKs and other unknown factors. Furthermore, dasatinib failed to suppress the pyroptosis induced by SPs with diameters of 50 and 100 nm (data not shown). Importantly, SPs of these sizes are internalized by phagocytosis and subsequently induce pyroptosis. Therefore, dasatinib-targeted SFKs may act on the downstream of specific particle receptors, facilitating the pyroptosis triggered by particles of specific sizes.

Microbial components adhere to the surfaces of externally invading particles [42-44]. The stimulation of pattern recognition receptors by microbial components, including TLR4, can induce an increase in and activate dasatinib-targeted SFKs (Figure 11). In addition, pattern recognition receptor activation induces the expression of inflammatory mediators, including IL-1α (Figure 11). These effects may

synergistically elevate the inflammatory responses triggered by pyroptosis on exposure to exogenously generated particles. I also demonstrated that LPS priming enhanced SP-induced cell death and IL-1α release. Importantly, SFK inhibition by dasatinib strongly suppressed SP-induced pyroptosis, including enhancement by LPS priming. My study results suggest that dasatinib-targeted SFKs mediate particle-induced phagolysosomal dysfunction, an early upstream event resulting in cell death; therefore, they are critical in determining the intensity of inflammation associated with particle-induced pyroptosis. As a result, SFK inhibition could be an effective and rational approach to prevent excessive inflammation caused by particles. This approach could be applicable for treating various particle-induced diseases since dasatinib suppresses pyroptosis induced by particles of various sizes and materials.

Moreover, I demonstrated that dasatinib treatment effectively ameliorated inflammatory manifestations in SP-induced acute lung injury in mice, characterized by the increased levels of IL-1α, IL-1β, CXCL1 and neutrophils. Importantly, the clinically relevant intragastric administration of dasatinib remarkably suppressed the SP-induced pulmonary inflammation and was as effective as its pulmonary administration. Neutrophils play an important role in acute lung injury after the inhalation of particle irritants [18]. Therefore, the oral administration of dasatinib can be used as an emergency measure to alleviate acute lung injury induced by the inhalation of particle irritants. In general, SFKs are multifunctional enzymes; therefore, the use of SFK inhibitors, such as dasatinib, in clinical settings is currently limited to treating cancers, such as chronic myeloid leukemia [45]. The inhalation of particle irritants in humans causes pneumoconiosis, characterized by persistent inflammation often accompanied by lung cancer [46]. However, only palliative treatment exists for pneumoconiosis. IL-1α may promote the development of lung

cancer [47]. Furthermore, neutrophilic inflammation is involved in silica-induced lung cancer progression [48]. To expand the range of treatments with SFK inhibitors, including dasatinib, their application for treating pneumoconiosis-associated lung cancer may be promising, particularly in the context of this study. In addition, chronic inflammation associated with pneumoconiosis often causes fibrosis. Dasatinib treatment is known to be effective in suppressing SP-induced pulmonary fibrosis [49]. Considering that IL-1 is involved in the development of SP-induced pulmonary fibrosis [50], the suppression of pyroptosis by dasatinib may contribute to its anti-fibrotic efficacy. The continuous intake of SFK inhibitors would be required to suppress chronic inflammation associated with pneumoconiosis and prevent lung carcinogenesis and fibrosis. In future, identifying SFKs that destabilize phagolysosomal membranes and their target molecules will aid in the development of more efficient, specific, and safe drugs for particle-induced inflammatory disease.

5. References

1. Bergsbaken, T., S.L. Fink, and B.T. Cookson, Pyroptosis: host cell death and inflammation. *Nat Rev Microbiol.*, 2009. **7**(2): p. 99-109.
2. Rao, Z., et al., Pyroptosis in inflammatory diseases and cancer. *Theranostics*, 2022. **12**(9): p. 4310-4329.
3. Dostert, C., et al., Innate immune activation through Nalp3 inflammasome sensing of asbestos and silica. *Science*, 2008. **320**(5876): p. 674-677.
4. Kuroda, E., et al., Inhaled fine particles induce alveolar macrophage death and interleukin-1α release to promote inducible bronchus-associated lymphoid tissue formation. *Immunity*, 2016. **45**(6): p. 1299-1310.
5. Cho, W.-S., et al., Inflammatory mediators induced by intratracheal instillation of ultrafine amorphous silica particles. *Toxicol. Lett.*, 2007. **175**(1-3): p. 24-33.
6. Yazdi, A.S., et al., Nanoparticles activate the NLR pyrin domain containing 3 (Nlrp3) inflammasome and cause pulmonary inflammation through release of IL-1α and IL-1β. *Proc. Natl. Acad. Sci. U S A.*, 2010. **107**(45): p. 19449-19454.
7. Palomaki, J., et al., Long, needle-like carbon nanotubes and asbestos activate the NLRP3 inflammasome through a similar mechanism. *ACS nano*, 2011. **5**(9): p. 6861-6870.
8. Martinon, F., et al., Gout-associated uric acid crystals activate the NALP3 inflammasome. *Nature*, 2006. **440**(7081): p. 237-241.
9. Duewell, P., et al., NLRP3 inflammasomes are required for atherogenesis and activated by cholesterol crystals. *Nature*, 2010. **464**(7293): p. 1357-1361.
10. Mulay, S.R., et al., Calcium oxalate crystals induce renal inflammation by NLRP3-mediated IL-1β secretion. *J. Clin. Invest.* , 2012. **123**(1).

11. Halle, A., et al., The NALP3 inflammasome is involved in the innate immune response to amyloid-β. *Nat. Immunol.*, 2008. **9**(8): p. 857-865.

12. Kinchen, J.M. and K.S. Ravichandran, Phagosome maturation: going through the acid test. *Nat. Rev. Mol. Cell Biol.*, 2008. **9**(10): p. 781-795.

13. Hornung, V., et al., Silica crystals and aluminum salts activate the NALP3 inflammasome through phagosomal destabilization. *Nat. Immunol.*, 2008. **9**(8): p. 847-856.

14. Yang, Y., et al., Recent advances in the mechanisms of NLRP3 inflammasome activation and its inhibitors. *Cell Death Dis.*, 2019. **10**(2): p. 128.

15. Groß, O., et al., Inflammasome activators induce interleukin-1α secretion via distinct pathways with differential requirement for the protease function of caspase-1. *Immunity*, 2012. **36**(3): p. 388-400.

16. Rabolli, V., et al., The alarmin IL-1α is a master cytokine in acute lung inflammation induced by silica micro-and nanoparticles. *Part. Fibre Toxicol.*, 2014. **11**(1): p. 1-15.

17. Rashidi, M., et al., The pyroptotic cell death effector gasdermin D is activated by gout-associated uric acid crystals but is dispensable for cell death and IL-1β release. *J. Immunol.*, 2019. **203**(3): p. 736-748.

18. Ikoma, K., et al., Oridonin suppresses particulate-induced NLRP3-independent IL-1α release to prevent crystallopathy in the lung. *Int. Immunol.*, 2022. **34**(10): p. 493-504.

19. Matsui, Y., et al., Nanaomycin E inhibits NLRP3 inflammasome activation by preventing mitochondrial dysfunction. *Int. Immunol.*, 2022. **34**(10): p. 505-518.

20. Pelegrin, P., C. Barroso-Gutierrez, and A. Surprenant, P2X7 receptor

differentially couples to distinct release pathways for IL-1β in mouse macrophage. *J. Immunol.*, 2008. **180**(11): p. 7147-7157.

21. Parsons, S.J. and J.T. Parsons, Src family kinases, key regulators of signal transduction. *Oncogene*, 2004. **23**(48): p. 7906-7909.
22. Byeon, S.E., et al., The role of Src kinase in macrophage-mediated inflammatory responses. *Mediators Inflamm.*, 2012. **2012**.
23. Kayagaki, N., et al., NINJ1 mediates plasma membrane rupture during lytic cell death. *Nature*, 2021. **591**(7848): p. 131-136.
24. Araujo, J. and C. Logothetis, Dasatinib: a potent SRC inhibitor in clinical development for the treatment of solid tumors. *Cancer Treat. Rev.*, 2010. **36**(6): p. 492-500.
25. Boggon, T.J. and M.J. Eck, Structure and regulation of Src family kinases. *Oncogene*, 2004. **23**(48): p. 7918-7927.
26. Maa, M.C. and T.H. Leu, Src is required for migration, phagocytosis, and interferon beta production in Toll-like receptor-engaged macrophages. *Biomedicine (Taipei)*, 2016. **6**(3): p. 14.
27. Kusaka, T., et al., Effect of silica particle size on macrophage inflammatory responses. *PloS one*, 2014. **9**(3): p. e92634.
28. Nishijima, N., et al., Human scavenger receptor A1-mediated inflammatory response to silica particle exposure is size specific. *Front. Immunol.*, 2017. **8**: p. 379.
29. Chen, C., et al., Monosodium urate crystals with controlled shape and aspect ratio for elucidating the pathological progress of acute gout. *Biomater. Adv.*, 2022. **139**: p. 213005.
30. Suzuki, T., et al., Differential involvement of Src family kinases in Fcγ

receptor-mediated phagocytosis. *J. Immunol.*, 2000. **165**(1): p. 473-482.

31. Uchimoto, T., et al., Mechanism of apoptosis induced by a lysosomotropic agent, L-Leucyl-L-Leucine methyl ester. *Apoptosis*, 1999. **4**: p. 357-362.

32. Majeed, M., et al., Role of Src kinases and Syk in Fcγ receptor-mediated phagocytosis and phagosome-lysosome fusion. *J. Leukoc. Biol.*, 2001. **70**(5): p. 801-811.

33. Scott, C.C., et al., Phosphatidylinositol-4, 5-bis phosphate hydrolysis directs actin remodeling during phagocytosis. *J. Cell Biol.*, 2005. **169**(1): p. 139-149.

34. Fehrenbacher, N., et al., Sensitization to the lysosomal cell death pathway by oncogene-induced down-regulation of lysosome-associated membrane proteins 1 and 2. *Cancer Res.*, 2008. **68**(16): p. 6623-6633.

35. Amaral, E.P., et al., Lysosomal cathepsin release is required for NLRP3-inflammasome activation by Mycobacterium tuberculosis in infected macrophages. *Front. Immunol.*, 2018. **9**: p. 1427.

36. Kumazoe, M., et al., Src Mediates Epigallocatechin-3-O-Gallate-Elicited Acid Sphingomyelinase Activation. *Molecules*, 2020. **25**(22).

37. Wähe, A., et al., Golgi-to-phagosome transport of acid sphingomyelinase and prosaposin is mediated by sortilin. *J. Cell Sci.*, 2010. **123**(14): p. 2502-2511.

38. Gault, C.R., L.M. Obeid, and Y.A. Hannun, An overview of sphingolipid metabolism: from synthesis to breakdown. *Adv. Exp. Med. Biol*, 2010. **688**: p. 1-23.

39. Boya, P. and G. Kroemer, Lysosomal membrane permeabilization in cell death. *Oncogene*, 2008. **27**(50): p. 6434-51.

40. Thibodeau, M.S., et al., Silica-induced apoptosis in mouse alveolar macrophages is initiated by lysosomal enzyme activity. *Toxicol. Sci.*, 2004.

80(1): p. 34-48.

41. Biswas, R., et al., Imipramine blocks acute silicosis in a mouse model. *Part. Fibre. Toxicol.*, 2017. **14**(1): p. 36.

42. Reed, C.E. and D.K. Milton, Endotoxin-stimulated innate immunity: a contributing factor for asthma. *J. Allergy Clin. Immunol.*, 2001. **108**(2): p. 157-166.

43. Ichinose, T., et al., The effects of microbial materials adhered to Asian sand dust on allergic lung inflammation. *Arch. Environ. Contam. Toxicol.*, 2008. **55**: p. 348-357.

44. He, M., et al., Effects of two Asian sand dusts transported from the dust source regions of Inner Mongolia and northeast China on murine lung eosinophilia. *Toxicol. Appl. Pharmacol.*, 2013. **272**(3): p. 647-655.

45. Aguilera, D.G. and A.M. Tsimberidou, Dasatinib in chronic myeloid leukemia: a review. *Ther. Clin. Risk Manag*, 2009. **5**(2): p. 281-9.

46. Tsuda, T., et al., A meta-analysis on the relationship between pneumoconiosis and lung cancer. *J. Occup. Health.*, 1997. **39**(4): p. 285-294.

47. Chiu, J.W., et al., IL-1α Processing, Signaling and Its Role in Cancer Progression. *Cells*, 2021. **10**(1): p. 92.

48. Satpathy, S.R., et al., Crystalline silica-induced leukotriene B4-dependent inflammation promotes lung tumour growth. *Nat. Commun.*, 2015. **6**(1): p. 1-12.

49. Cruz, F.F., et al., Dasatinib Reduces Lung Inflammation and Fibrosis in Acute Experimental Silicosis. *PLoS One*, 2016. **11**(1): p. e0147005.

50. Piguet, P.F., et al., Interleukin 1 receptor antagonist (IL-1ra) prevents or cures pulmonary fibrosis elicited in mice by bleomycin or silica. *Cytokine*, 1993.

5(1): p. 57-61.

6. Acknowledgment

I would like to express my sincere gratitude to Professor Saitoh, Associate Professor Takemura, and Assistant Professor Takahama for their support and critiques throughout my research journey. Their insights and constructive criticism were vital at every stage of this project and thesis.

Secondly, I would like to thank the members of the Center for Supporting Drug Discovery and Life Science Research, Graduate School of Pharmaceutical Science, Osaka University. They kindly provide the compounds libraries and technical support in high-throughput screening.

Moreover, I would like to acknowledge the financial support of the Watanuki International Scholarship Foundation.

Furthermore, I want to thank the Laboratory of Bioresponse Regulation members for their help in my academic studies.

Finally, I want to thank my parents for their love and support. Without their support, their belief in me kept me going during the most challenging times, and I am forever indebted to them. I would also like to extend my heartfelt thanks to my friends, Mr. Xiao, Mr. Yan, and Mr. Zhou, for their unwavering support and encouragement during challenging times.

FIGURE 1

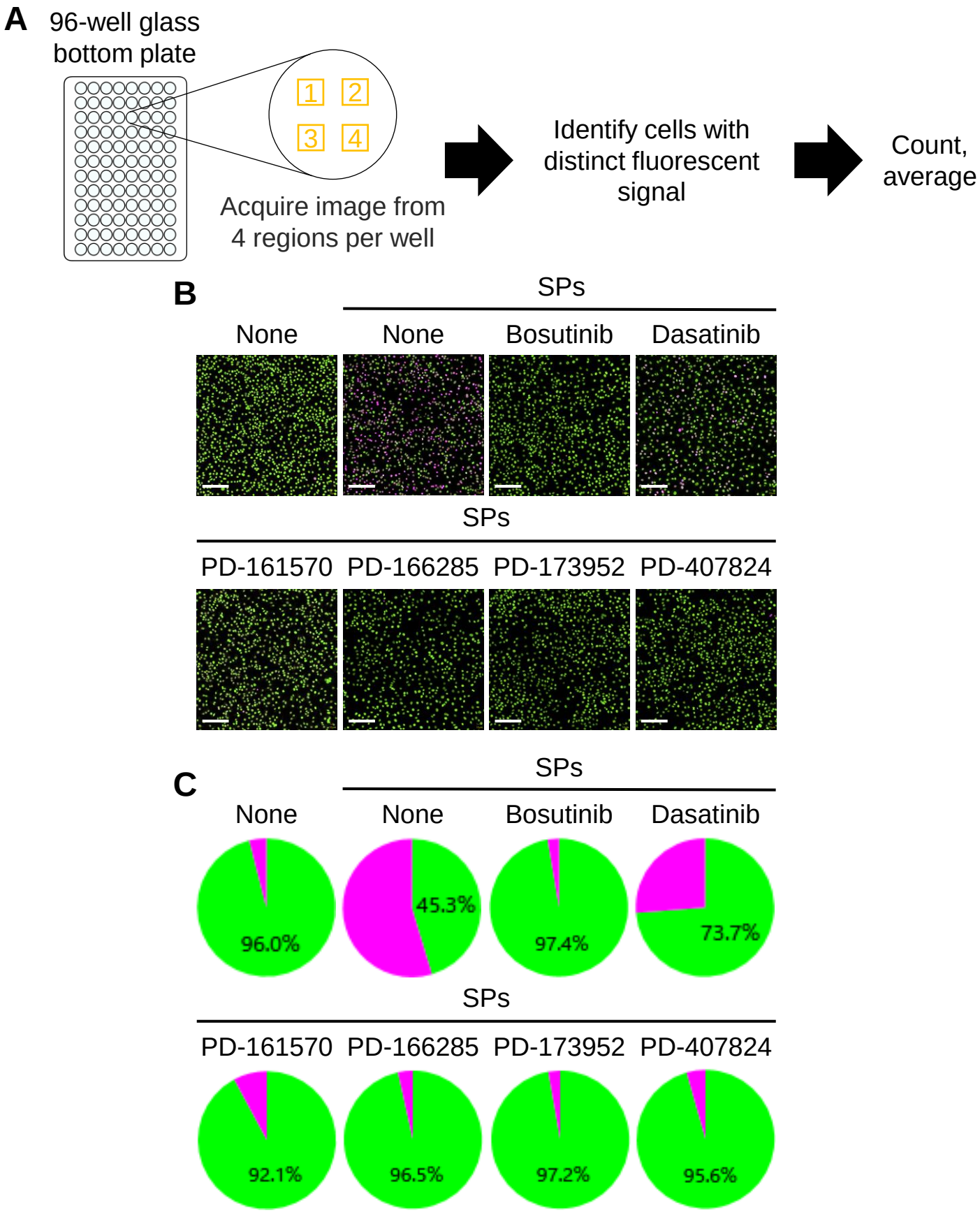
A
96-well glass bottom plate
1
2
3
4
Acquire image from 4 regions per well
Identify cells with distinct fluorescent signal
Count, average
B
SPs
None
None
Bosutinib
Dasatinib
SPs
PD-161570
PD-166285
PD-173952
PD-407824
C
SPs
None
None
Bosutinib
Dasatinib
96.0%
45.3%
97.4%
73.7%
SPs
PD-161570
PD-166285
PD-173952
PD-407824
92.1%
96.5%
97.2%
95.6%

FIGURE 1

FIGURE 1. Imaging-based high-throughput screening for compounds that inhibit silica particle (SP)-induced cell death. **(A)** The analysis procedure for the screening using CV8000. Lipopolysaccharide (LPS)-primed RAW264.7 cells were treated by each test compound (5 μM) from Pfizer drug and the Food and Drug Administration (FDA)-approved drug libraries for 30 min and then stimulated with SPs (500 nm in diameter, 500 μg/ml), in the presence of Hoechst 33342 (1 μg/ml, green) and DRAQ7 (2 μM, magenta) for 2 h. The images were acquired at four different fields in each well. Hoechst 33342-positive, DRAQ7-negative cells and Hoechst 33342 and DRAQ7 double-positive cells were regarded as viable cells and dead cells, respectively. **(B)** The representative images of the cells treated with hit compounds. Scale bar, 120 μm. **(C)** The rate of viable cells (green) and dead cells (magenta) of **(B)** was calculated by CellPathfinder software.

Table 1

Table 1. List of candidate drugs that inhibit silica particle-induced cell death accompanied by IL-1α release.

Stimulation	Candidate drugs	Cell death (%)	IL-1α (pg/ml)	References
None	-	4 ± 0.2	201.5 ± 0.7	-
Silica particles	-	54.1 ± 3	3192.7 ±36.2	-
	Bosutinib	3.3 ± 0.9	125.7 ± 35.4	Golas et al., 2003
	Dasatinib	26.6 ± 4	1262.7 ± 766.7	Lombardo et al., 2004
	PD-161570	7.9 ± 3.5	229.8 ± 0.1	Hamby et al., 1997
	PD-166285	4.5 ± 1.4	143 ± 4.2	Panek et al., 1997
	PD-173952	2.7 ± 1.3	718.4 ± 44.1	Dorsey et al., 2002
	PD-407824	4.4 ± 0.6	1524.5 ± 261.7	Palmer et al., 2006

FIGURE 2

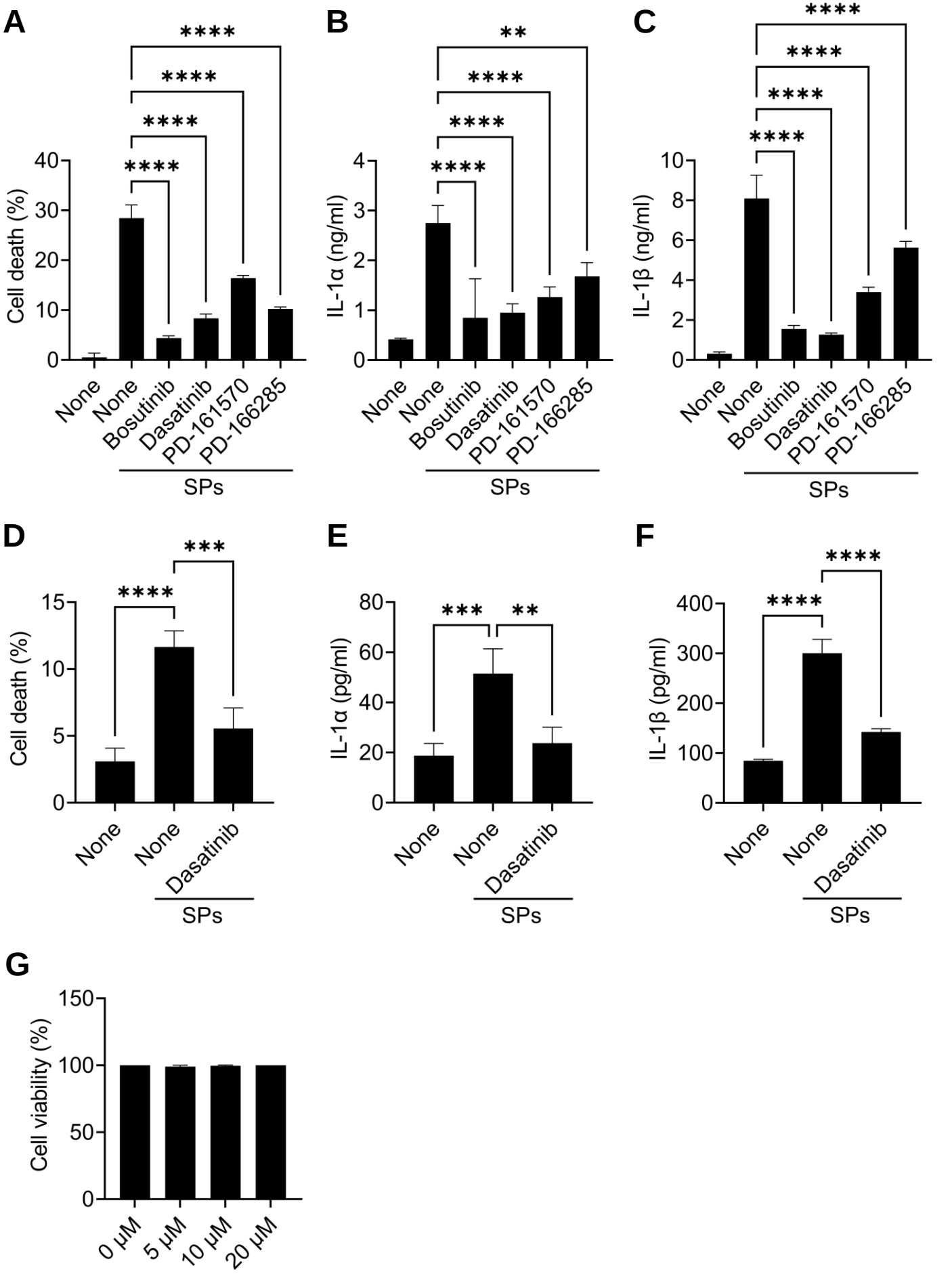
A
B
C
D
E
F
G
Cell death (%)
IL-1α (ng/ml)
IL-1β (ng/ml)
IL-1α (pg/ml)
IL-1β (pg/ml)
Cell viability (%)
None
None
Bosutinib
Dasatinib
PD-161570
PD-166285
SPs
0 μM
5 μM
10 μM
20 μM

FIGURE 2

FIGURE 2. Dasatinib suppresses silica particle (SP)-induced cell death accompanied by interleukin-1 alpha (IL-1α) release. **(A-C)** Bone marrow-derived macrophages (BMDMs) were primed with lipopolysaccharide (LPS) (200 ng/ml) for 6 h. The cells were then treated with bosutinib (20 μM), dasatinib (20 μM), PD-161570 (20 μM), and PD-166285 (20 μM) and were stimulated or not stimulated with SPs (1,500 nm in diameter, 300 μg/ml) for 2 h. **(A)** The cell death rate was determined by measuring lactate dehydrogenase (LDH) activity in the culture supernatants. **(B, C)** IL-1α and IL-1 beta (β) levels in the culture supernatants were measured using enzyme-linked immunosorbent assay (ELISA). **(D-F)** Phorbol 12-myristate 13-acetate-differentiated THP-1 cells were primed with LPS (50 ng/ml) for 16 h. The cells were then treated with dasatinib (20 μM) and were stimulated or not stimulated with SPs (1,500 nm in diameter, 500 μg/ml) for 4 h. **(D)** Cell death rate was determined by measuring LDH activity in the culture supernatants. **(E, F)** IL-1α and IL-1β levels in the culture supernatants were measured using ELISA. **(G)** BMDMs were treated with increasing doses of dasatinib (0–20 μM) for 12 h; thereafter, the cell death rate was determined by measuring LDH activity in the culture supernatants. The results are presented as the mean ± SD of values from triplicate wells. **, $P < 0.01$; ***, $P < 0.001$; and ****, $P < 0.0001$.

FIGURE 3

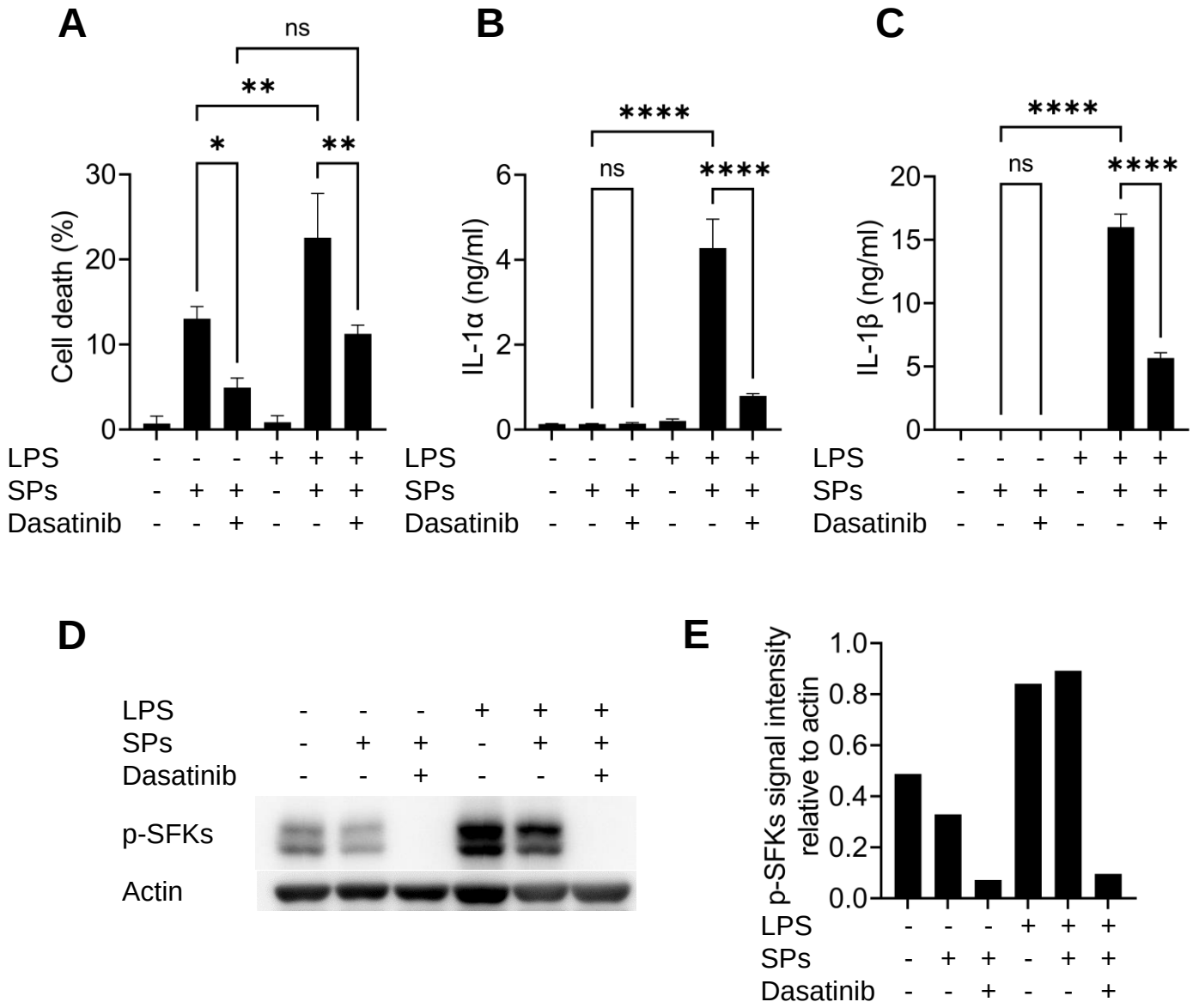

FIGURE 3. Lipopolysaccharide (LPS)-priming increases the levels of phosphorylated Src family kinases (p-SFKs) and enhances silica particle (SP)-induced pyroptosis. **(A-E)** Unprimed and LPS-primed bone marrow-derived macrophages (BMDMs) were treated with dasatinib (20 μM) and stimulated or not stimulated with SPs (1,500 nm in diameter, 300 μg/ml) for 2 h. **(A)** The cell death rate was determined by measuring lactate dehydrogenase (LDH) activity in the culture supernatants. **(B, C)** Interleukin-1 alpha (IL-1α) and IL-1 beta (β) levels in the culture supernatants were measured using enzyme-linked immunosorbent assay (ELISA). **(D)** Immunoblot analysis of p-SFKs in the cell extracts of BMDMs. **(E)** Quantification of p-SFK levels compared to actin control in each condition indicated in (**D**). The results are presented as the mean ± SD of values from triplicate wells. *, $P < 0.05$; **, $P < 0.01$; ****, $P < 0.0001$; and ns, not significant.

FIGURE 4

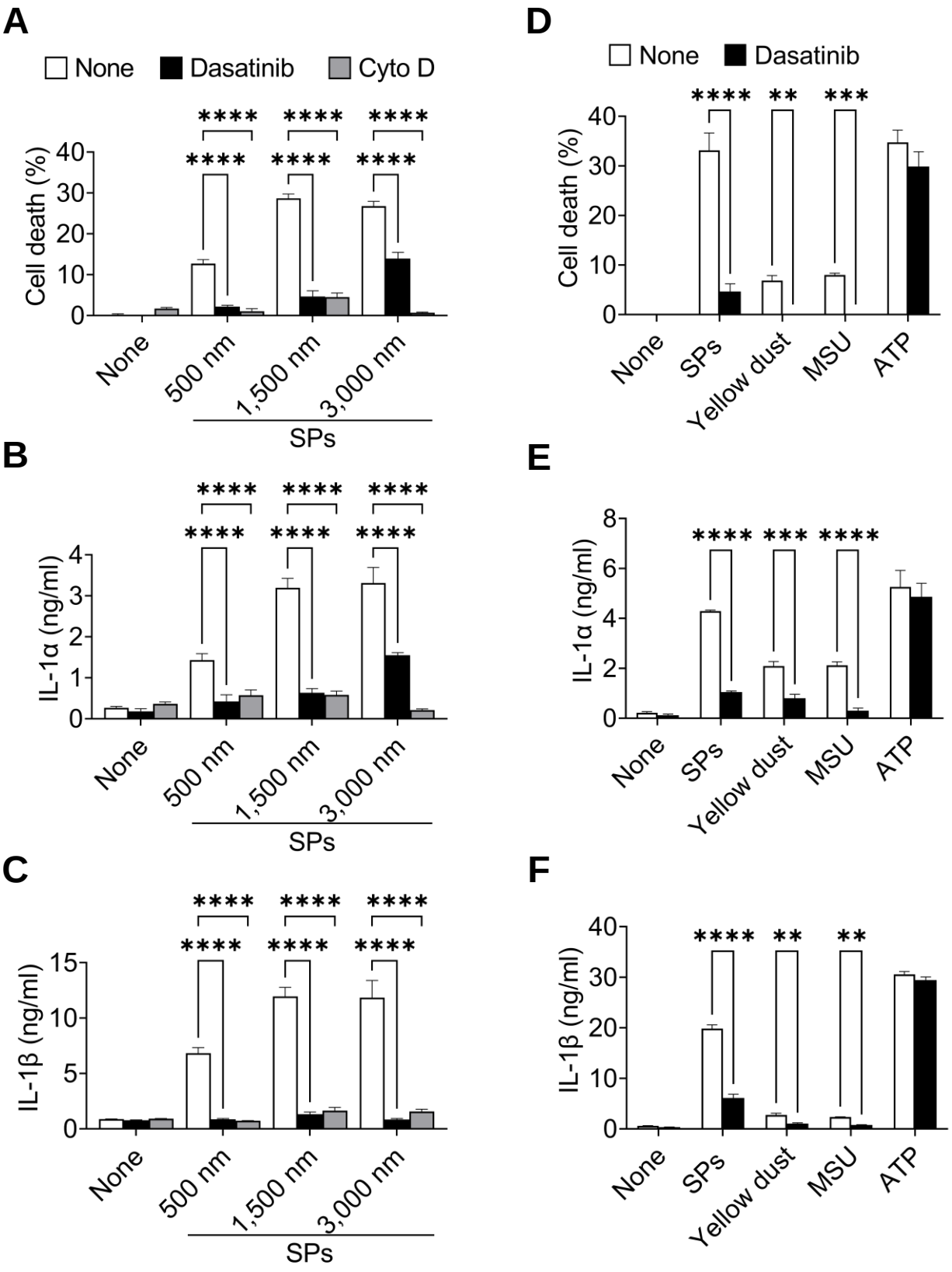
A
None
Dasatinib
Cyto D
Cell death (%)
****
None
500 nm
1,500 nm
3,000 nm
SPs
B
IL-1α (ng/ml)
C
IL-1β (ng/ml)
D
**
***
SPs
Yellow dust
MSU
ATP
E
F

FIGURE 4. Dasatinib suppresses pyroptosis induced by particles of various sizes or materials. **(A-C)** Primed bone marrow-derived macrophages (BMDMs) were treated with dasatinib (20 μM) or cytochalasin D (Cyto D) (20 μM) and stimulated or not stimulated with silica particles (SPs) (500, 1,500, or 3,000 nm in diameter, 300 μg/ml) for 2 h. **(A)** The cell death rate was determined by measuring lactate dehydrogenase (LDH) activity in the culture supernatants. **(B, C)** Interleukin-1 alpha (IL-1α) and IL-1 beta (β) levels in the culture supernatants were measured using enzyme-linked immunosorbent assay (ELISA). **(D-F)** Primed BMDMs were treated with dasatinib (20 μM) and stimulated or not stimulated with SPs (1,500 nm in diameter, 300 μg/ml), yellow dust (500 μg/ml), monosodium urate (MSU) (300 μg/ml) or adenosine triphosphate (ATP) (3 mM) for 2 h. **(D)** The cell death rate was determined by measuring LDH activity in the culture supernatants. **(E, F)** IL-1α and IL-1β levels in the culture supernatants were measured using ELISA. The results are presented as the mean ± SD of values from triplicate wells. **, $P < 0.01$; ***, $P < 0.001$; and ****, $P < 0.0001$.

FIGURE 5

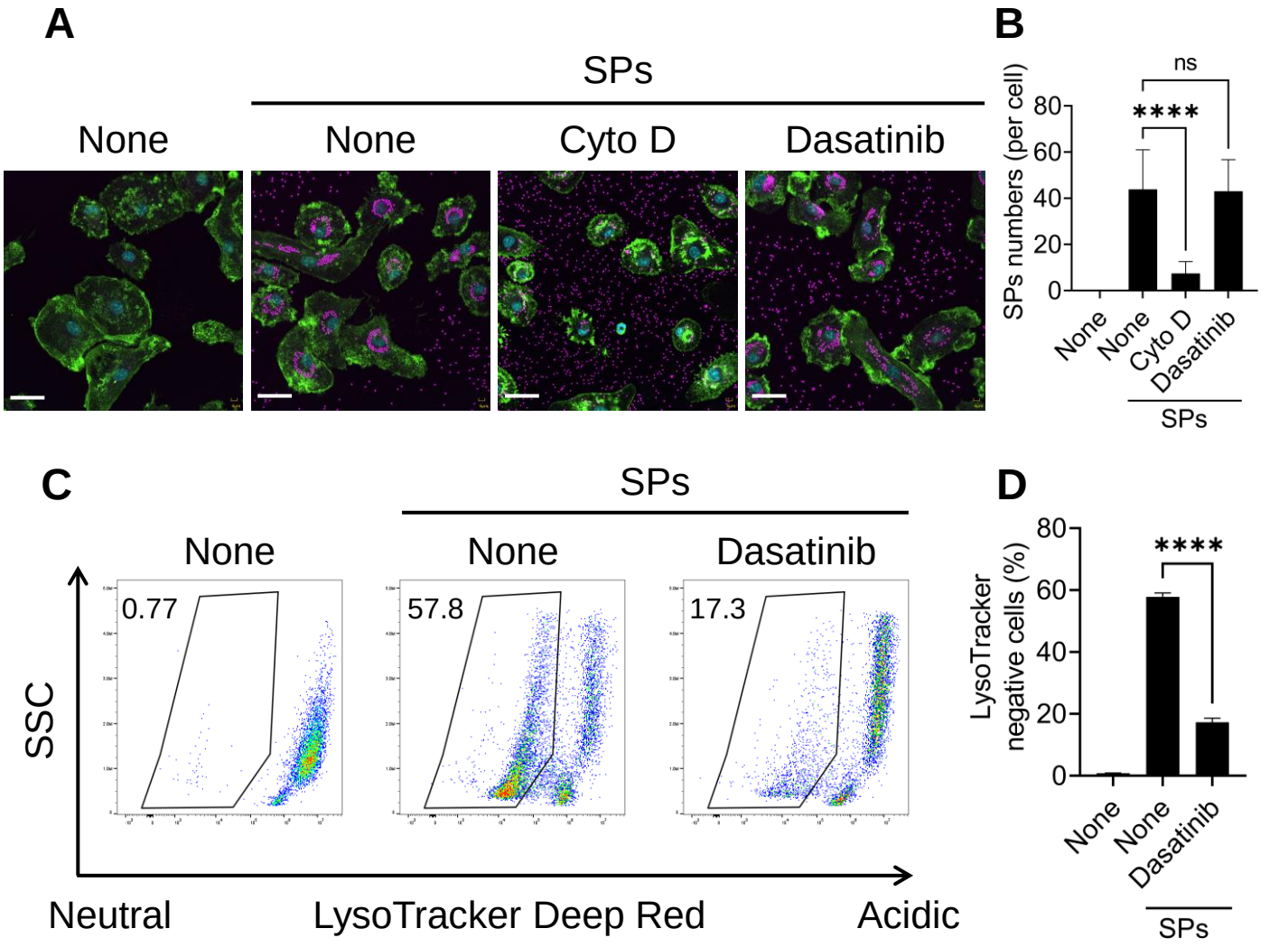

FIGURE 5. Dasatinib suppresses phagolysosomal dysfunction induced by silica particles (SPs). **(A)** Primed bone marrow-derived macrophages (BMDMs) were treated with 20 μM cytochalasin D (Cyto D) or dasatinib and stimulated or not stimulated with fluorescent SPs (1,500 nm in diameter, 20 μg/ml; magenta) for 2 h. Actin (green) and nuclei (cyan) were stained with phalloidin and DRAQ5, respectively. Scale bar; 30 μm. **(B)** Numbers of SPs in BMDMs. The results are presented as the mean ± SD of values from 74 cells. **(C)** Flow cytometric analysis of the primed BMDMs treated with dasatinib (20 μM) and stimulated or not stimulated with SPs (1,500 nm in diameter, 300 μg/ml) for 2 h. The cells were stained with the fluorescent dye LysoTracker Deep Red. The data are representative of three independent experiments. **(D)** Percentages of the LysoTracker Deep Red-negative population were calculated. The results are presented as the mean ± SD of values from triplicate wells. ****, $P < 0.0001$; and ns, not significant.

FIGURE 6

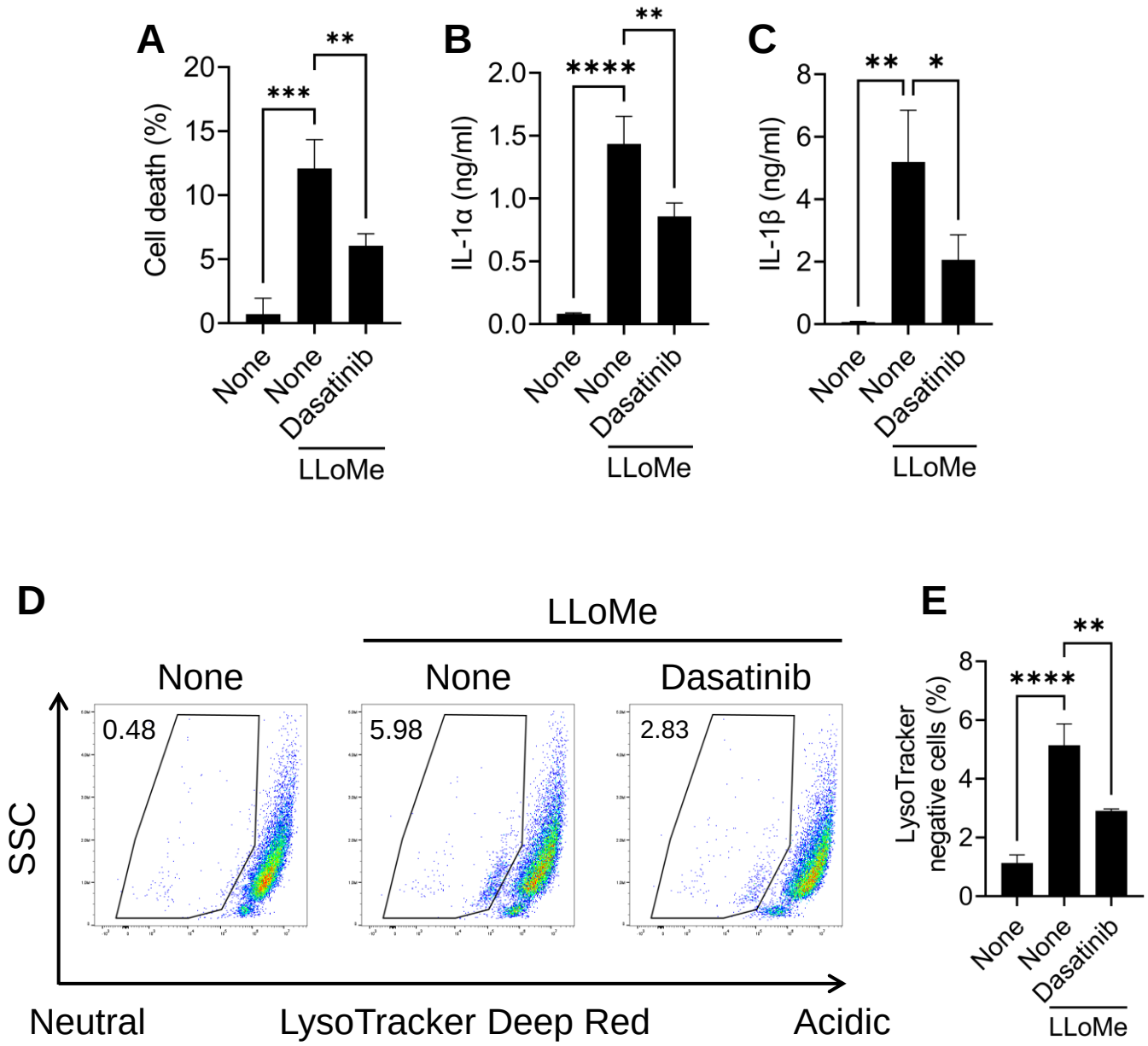

FIGURE 6. Dasatinib suppresses L-leucyl-L-leucine methyl ester (LLoMe)-induced lysosomal dysfunction and subsequent pyroptosis. **(A-C)** Primed BMDMs were treated with dasatinib (20 μM) and left unstimulated or stimulated with LLoMe (0.5 mM) for 3 h. **(A)** The cell death rate was determined by measuring lactate dehydrogenase (LDH) activity in the culture supernatants. **(B, C)** Interleukin-1 alpha (IL-1α) and IL-1 beta (β) levels in the culture supernatants were measured using enzyme-linked immunosorbent assay (ELISA). **(D)** Flow cytometric analysis of primed BMDMs treated with dasatinib (20 μM) and stimulated or not stimulated with LLoMe (0.5 μM) for 3 h. The cells were stained with the fluorescent dye LysoTracker Deep Red. The data are representative of three independent experiments. **(E)** Percentages of the LysoTracker Deep Red-negative population were calculated. The results are presented as the mean ± SD of values from triplicate wells. *, $P < 0.05$; **, $P < 0.01$; ***, $P < 0.001$; and ****, $P < 0.0001$.

FIGURE 7

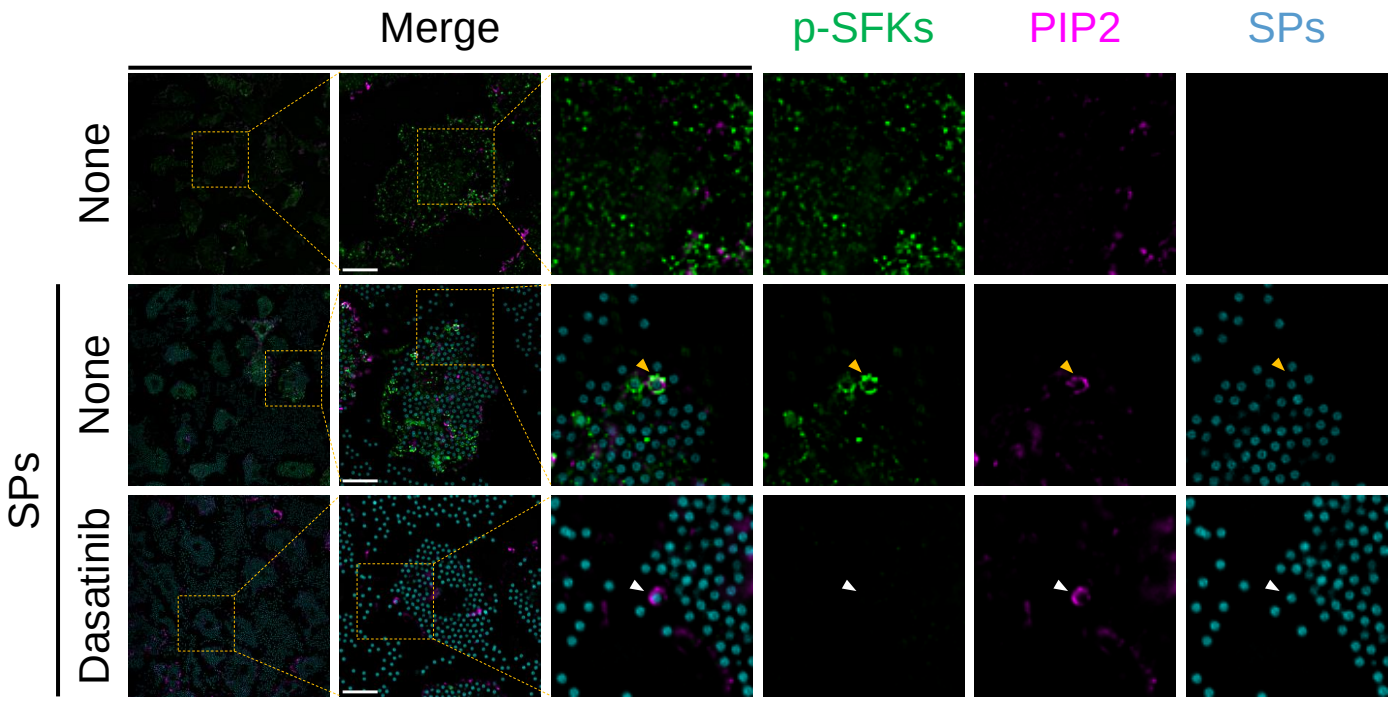

FIGURE 7. Phosphorylated Src family kinases (p-SFKs) accumulate around silica particle (SP)-containing phagocytic cups shortly after the phagocytosis of SPs. Primed bone marrow-derived macrophages (BMDMs) were treated with dasatinib (20 μM) and stimulated or not stimulated with fluorescent SPs (1,500 nm in diameter, 300 μg/ml; cyan). 15 min after stimulation with fluorescent SPs, p-SFKs (green) and phosphatidylinositol 4,5-bisphosphate (PIP2) (magenta) were stained with specific antibodies. The white arrowhead indicates SP surrounded by PIP2. Yellow arrowheads indicate SPs surrounded by both p-SFKs and PIP2. Scale bar; 10 μm.

FIGURE 8

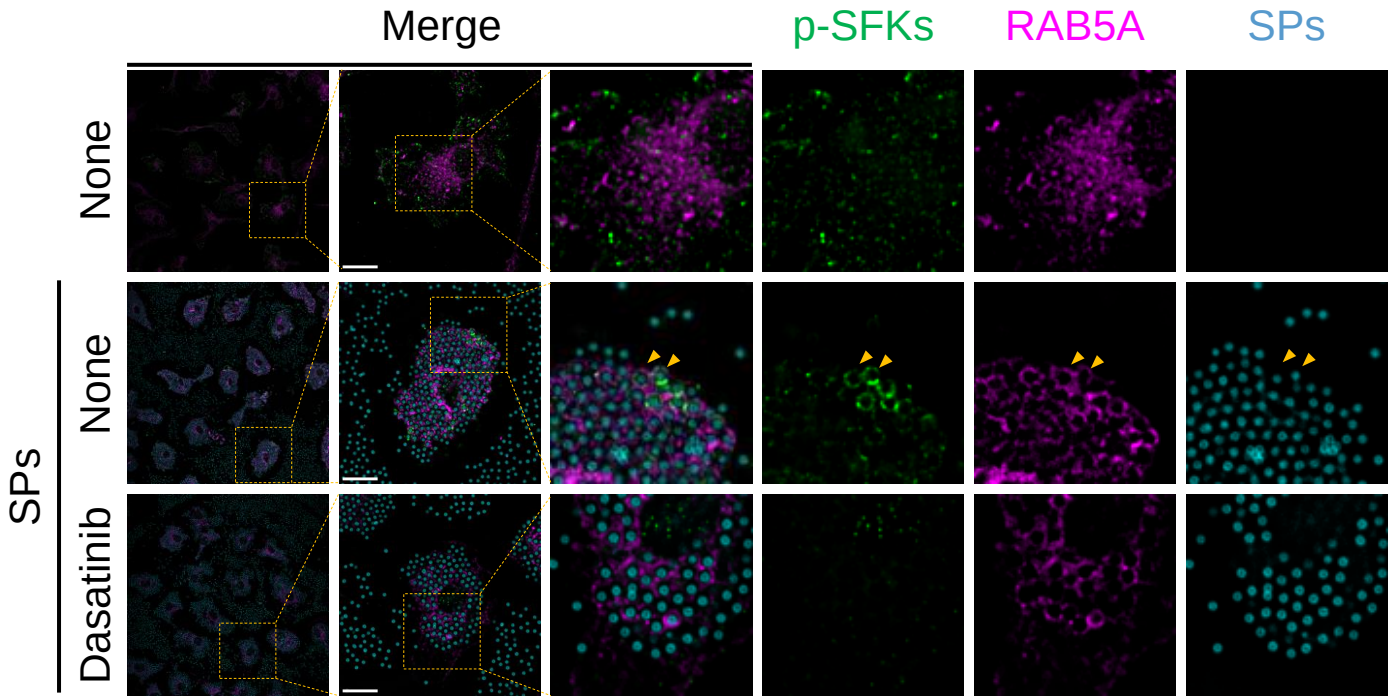

FIGURE 8. Phosphorylated Src family kinases (p-SFKs) accumulate around silica particle (SP)-containing early phagosomes. Primed bone marrow-derived macrophages (BMDMs) were treated with dasatinib (20 μM) and stimulated or not stimulated with fluorescent SPs (1,500 nm in diameter, 300 μg/ml; cyan). 30 min after stimulation with fluorescent SPs, p-SFKs (green) and RAB5A, member RAS oncogene family (RAB5A) (magenta) were stained with specific antibodies. Yellow arrowheads indicate SPs surrounded by both p-SFKs and RAB5A. Scale bar; 10 μm.

FIGURE 9

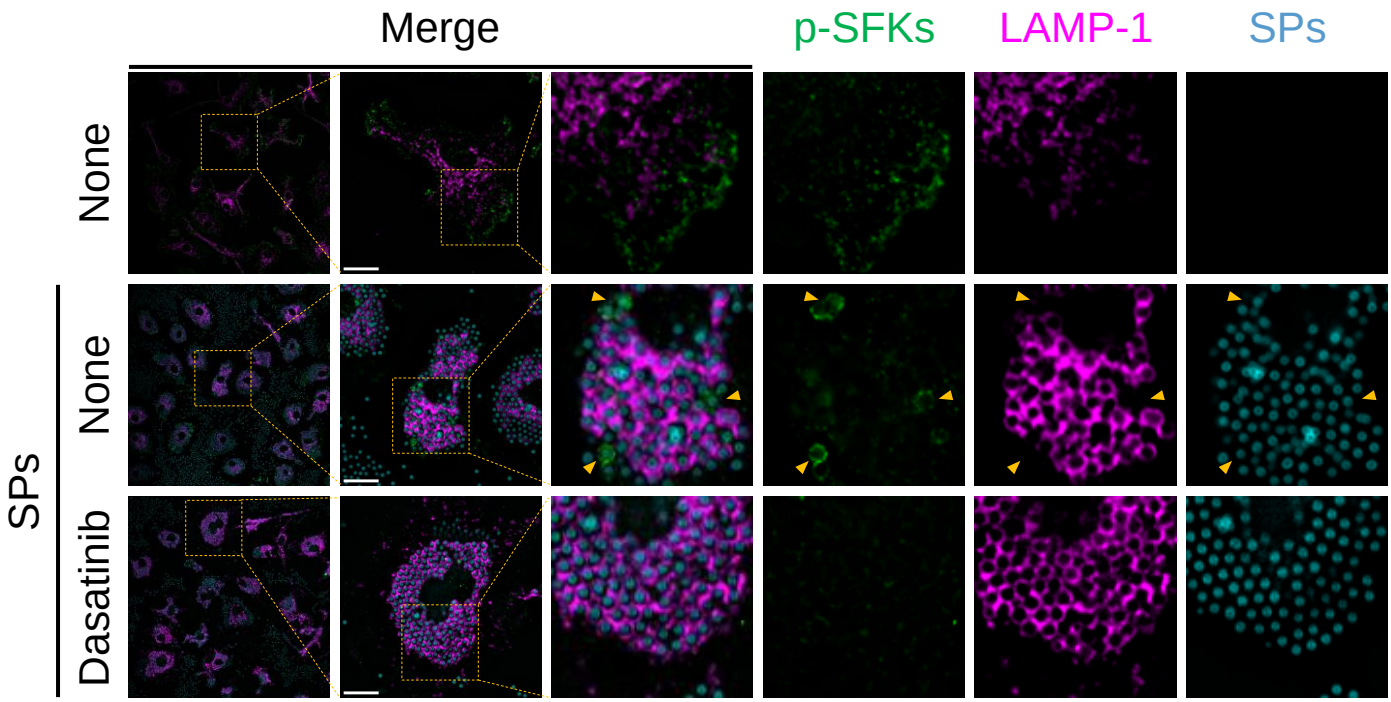

FIGURE 9. Silica particle (SP)-containing phagosomes are surrounded by phosphorylated Src family kinases (p-SFKs) but not lysosome-associated membrane protein-1 (LAMP-1). Primed bone marrow-derived macrophages (BMDMs) were treated with dasatinib (20 μM) and stimulated or not stimulated with fluorescent SPs (1,500 nm in diameter, 300 μg/ml; cyan). 30 min after stimulation with fluorescent SPs, p-SFKs (green), and LAMP-1 (magenta) were stained with specific antibodies. Yellow arrowheads indicate p-SFK-surrounded SPs. Scale bar; 10 μm.

FIGURE 10

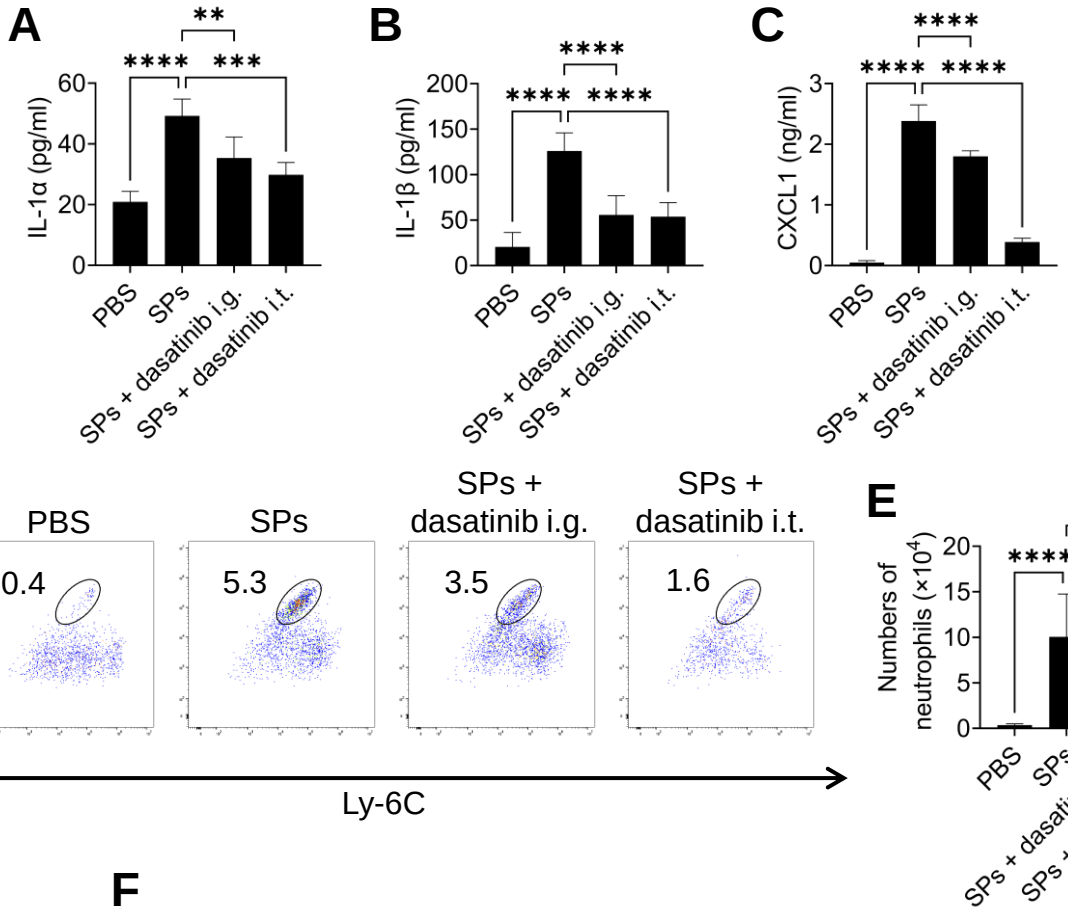
A
B
C
IL-1α (pg/ml)
IL-1β (pg/ml)
CXCL1 (ng/ml)
PBS
SPs
SPs + dasatinib i.g.
SPs + dasatinib i.t.

D
PBS
SPs
SPs + dasatinib i.g.
SPs + dasatinib i.t.
0.4
5.3
3.5
1.6
Ly-6G
Ly-6C

E
Numbers of neutrophils (×10⁴)
PBS
SPs
SPs + dasatinib i.g.
SPs + dasatinib i.t.

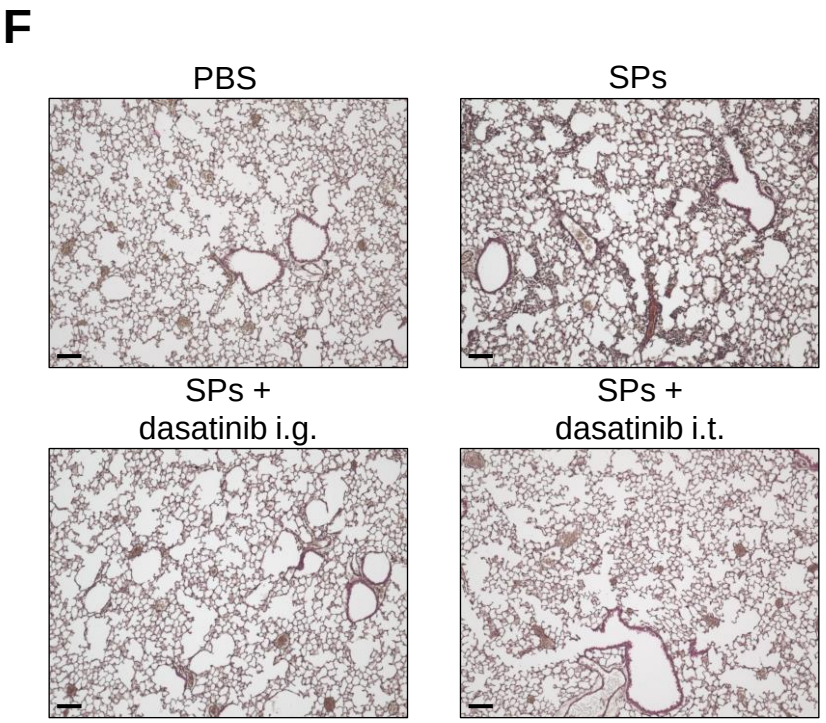
F
PBS
SPs
SPs + dasatinib i.g.
SPs + dasatinib i.t.

FIGURE 10

FIGURE 10. Dasatinib treatment alleviates silica particle (SP)-induced acute pneumonia. **(A-C)** Bronchoalveolar lavage (BAL) fluid was collected from mice 12 h after intratracheal SP administration (i.t.; 100 mg/kg) with or without the intragastric (i.g.; 30 mg/kg) and intratracheal (10 mg/kg) administration of dasatinib. Interleukin-1 alpha (IL-1α), IL-1 beta (β), and chemokine (C-X-C motif) ligand 1 (CXCL1) levels in the BAL fluid were measured using enzyme-linked immunosorbent assay (ELISA). **(D)** Neutrophils in mouse lungs 12 h after intratracheal SP administration were counted using flow cytometry. The numbers in the plots indicate the percentage of neutrophils in total leukocytes. **(E)** The total number of neutrophils. **(F)** Representative images of hematoxylin and eosin staining of mouse lungs were collected 12 h after intratracheal SP administration. Scale bar; 100 μm. The results are presented as mean ± SD (n = 5, each group). **, $P < 0.01$; ***, $P < 0.001$; and ****, $P < 0.0001$.

FIGURE 11

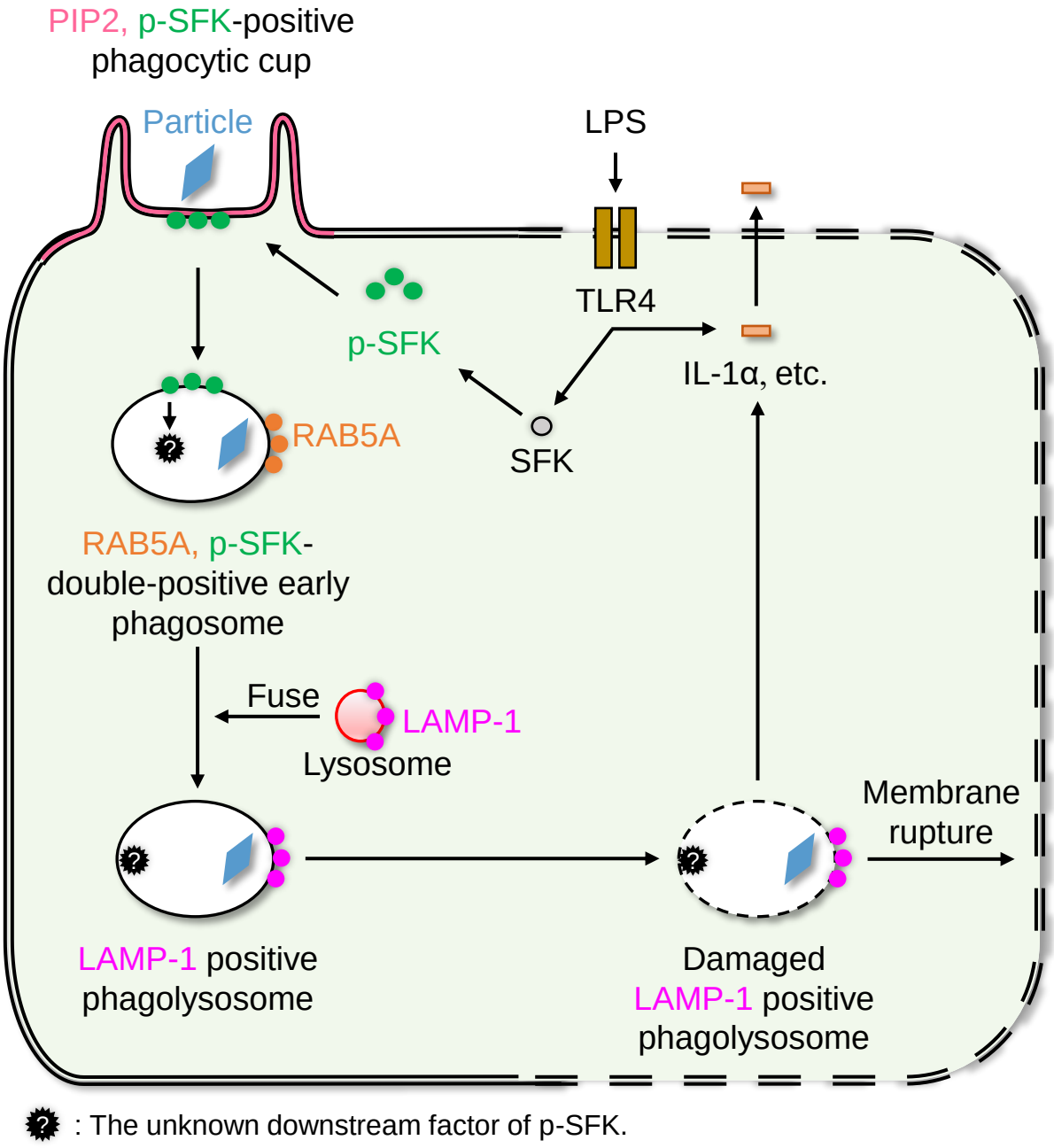

FIGURE 11. Phosphorylated Src family kinases (p-SFKs) facilitate the destabilization of phagolysosomes, thereby inducing pyroptosis. Toll-like receptor 4 (TLR4) activation induces an increase in and activates SFKs, and induces the expression of inflammatory mediators, including interleukin-1 alpha (IL-1α). After being stimulated by particles, p-SFKs accumulate around the phosphatidylinositol 4,5-bisphosphate (PIP2)-positive phagocytic cups formed immediately after the phagocytosis of particles. p-SFKs persist on RAB5A, member RAS oncogene family (RAB5A)-positive early phagosomes. Thereafter, phagosomes become lysosome-associated membrane protein-1 (LAMP-1)-positive phagolysosomes after fusing with lysosomes. Finally, the damaged phagolysosomes induce plasma membrane rupture and the release of IL-1α and other inflammatory mediators. However, p-SFKs do not accumulate around the LAMP-1-positive phagolysosomes. Therefore, it is presumed that p-SFKs may facilitate the membrane destabilization of phagosomes and/or phagolysosomes that engulf particles via an unknown downstream factor.